Renewable Energy 222 (2024) 119899

Contents lists available at ScienceDirect

Renewable Energy

journal homepage: www.elsevier.com/locate/renene

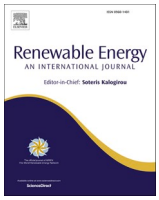

High-temperature high-pressure electrochemical hydrogenation of biocrude oil

Primavera Pelosin [a], Francesco Longhin [b], Nikolaj Bisgaard Hansen [a], Paolo Lamagni [c], Emil Drazevic [a], Patricia Benito [d], Konstantinos Anastasakis [a], Jacopo Catalano [a,*]

[a] Department of Biological and Chemical Engineering, Aarhus University, Aabogade 40, DK-8200, Aarhus N, Denmark
[b] Department of Physics, Technical University of Denmark, Fysikvej, DK-2800, Kgs. Lyngby, Denmark
[c] Advanced Surface Plating ApS, Axel Gruhns Vej 3, 8270, Højbjerg, Denmark
[d] Department of Industrial Chemistry "Toso Montanari", Viale Del Risorgimento 4, 40136, Bologna, Italy

ARTICLE INFO

Keywords:
Biocrude from hydrothermal liquefaction
High-temperature
In-situ partial upgrading
Membrane-less electrochemistry

ABSTRACT

Hydrothermal liquefaction (HTL) occurs at high pressures (160–200 bar) and temperatures (300–350 °C), where the conditions in the reactor drive the conversion of wet biomass to biocrude oil (BC). Before drop-in, BC needs further upgrading (hydrogenation) to increase the energy content and decrease the concentration of heteroatoms. Normally this is done in hydrogenation reactors at high pressures and temperatures, which require an external high pressure H_2 source. The main HTL by-product is process water (PW), which is either recirculated or cleaned before being disposed. Herein we investigated a membrane-less electrochemical method, which uses PW as hydrogen source and can be seamlessly integrated in HTL plants. We demonstrate a *proof-of concept* of a membrane-less electrochemical reactor that oxidizes PW at the anode and uses hydrogen in form of protons and electrons to hydrogenate BC at the cathode. We report BC upgrading (atomic H/C ratio increase up to 17 %) at high-pressure (up to 100 bar) and high-temperature (up to 200 °C), which mimic the conditions of an actual HTL plant. The *proof-of-concept* discussed here is a novel way of increasing the hydrogen content of biocrude oil within HTL reactor by using electricity, with no need of an external high-pressure H_2 source.

1. Introduction

Due to the continuous demographic and economic growth, the world demand for energy is increasing, while fossil fuel reservoirs are depleting. Besides from their finite nature, fossil fuels are one of the major causes of greenhouse gases, since their combustion, generates CO_2 along with other harmful substances [1]. During the past decades, research focused on finding renewable and sustainable sources of energy, and major advances were achieved in advancing and deploying technologies for generation of electricity from wind and solar energy [2].

Direct electrification and use of batteries can decarbonize much of the transport sector, however long-distance heavy transport, such as trucks, ships and airplanes, is foreseen to rely on liquid fuels in the middle- and long-term future [3]. A tremendous effort is therefore required to find a sustainable "green" replacement of liquid fossil fuels. Biomass, such as organic waste streams, is advanced as a possible substitute [4,5] and hydrothermal liquefaction (HTL) is one of the most promising technologies for converting organic materials into synthetic petroleum crude oil. HTL mimics the natural process of petroleum formation on earth, accelerating the timescale from millions of years to minutes by applying high pressure (160–200 bar) and temperature (300–350 °C). The conversion happens in the presence of H_2O and is applicable to any type of biomass that can be suspended in water. The main HTL product is bio-crude (BC), a replacement to petroleum crude oil with high heating value (~30–40 MJ kg^{-1}), which can be integrated in the existing petroleum infrastructures [6–8]. Nevertheless, before drop-in, BC must match the physicochemical properties of petroleum crude oil, and for this reason it needs a chemical upgrade. The upgrade should significantly reduce the total acidity number and a deep heteroatom fraction (mostly oxygen and nitrogen), to increase the bio-oil's heating value and stability. Furthermore, the high content of reactive compounds makes challenging the storage and transport of the bio-crude oil and a fast *in-situ* upgrade could avoid, or at least slow down, the crude oil decay [9,10]. Bio-oils upgrade therefore principally targets to increase the H/C ratio over the O/C ratio, which ultimately

* Corresponding author.
E-mail address: jcatalano@au.dk (J. Catalano).

https://doi.org/10.1016/j.renene.2023.119899
Received 10 July 2023; Received in revised form 23 November 2023; Accepted 25 December 2023
Available online 28 December 2023

results in fuels with higher heating values [11]. Traditional catalytic oil hydrogenation normally occurs via $NiMo/Al_2O_3$ catalyst at $T =$ 350–400 °C, $p =$ 40–180 bar and a very effective mixing with hydrogen gas. These hydrogenation methods are costly, occur at severe operative conditions, and require a separate reactor for heterogeneous catalysis. Additionally, the H_2 at high pressure needed is normally produced elsewhere and transported to the hydrogenation facility [9].

Traditional oil hydrogenation can be replaced with a milder electrocatalytic hydrogenation (ECH). ECH can work at ambient conditions in terms of pressure and temperature, and it needs just electricity and a proton/electron source (*e.g.* water) to upgrade BC oils; therefore, it is suitable for use in delocalised plants and can help the coupling of biocrude refining and renewable electricity obtained from sun or wind [12]. So far the studies in this field dealt prevalently with model compounds such as aldehydes (benzaldehyde [13,14] and furfurals [15–18]) ketones [14] and phenols [14,19–21]. Other works performed electrolysis in oils derived from pyrolysis [22–27], often treating the water soluble [22,24] and the hydrophobic [24,25] fractions separately. These works were successful in proving the electrochemical reduction of oxygenated compound to molecule of higher calorific value once the right conditions such as the applied voltage and the type of catalyst were selected. In any case, such studies mostly focussed on replacing traditional hydrogenation reactors with an *ex-situ* electrochemical reactor. Therefore, they partially solved the problem of using milder conditions for bio-oil upgrading but were not able to reduce the number of unit operations.

In this study we advance the *state-of-the-art* by considering a novel approach, which allows for an *in situ* ECH. Here we use the case study of an HTL loop, since its reactor contains process water (PW), which is the ideal source of protons and electrons. PW represents the largest fraction of the outlet stream of the HTL reactor, since to pump the biomass, it must be suspended in water in the ratio of around 1:5. PW contains high concentrations of organic and inorganic compounds [28,29] and, as such, must be either recirculated to the HTL reactor (when starting from relatively dry feedstocks *e.g.* lignocellulose biomass) or treated before disposal (when starting from wet feedstocks *e.g.* in the case of sewage sludge from waste water treatment plants). In addition, the high operating pressure employed in HTL, necessitates the investigation of ECH at elevated pressures, hence further advancing the *state-of-the-art* which until now had dealt with ECH only at ambient pressure.

In this study we performed ECH at HTL working conditions, using actual biocrude oil produced in the HTL facilities at Foulum, Denmark. At high temperatures and pressures (similar to those in the HTL reactor), the biocrude oil is believed to form a two-phase water-oil immiscible mixture. This opens an electrochemical route to produce hydrogen in the form of protons and electrons at the anolyte, where water can be split. Due to the electrical applied potential, an electric field is created, and produced protons then electro-migrate through the solution to the catholyte (BC phase), while electrons move through the wire to the cathode, to electrochemically hydrogenate the oil phase. The proposed method has the advantage of hydrogenating the produced BC *in situ*, without the need of an additional post-processing unit and without the use of any separator (*e.g.* high temperature membranes). The present work aims to answer the following research questions; Q1 Is direct BC-ECH at high-pressure and high temperature possible? Q2 Can the immiscibility of the oil-water phases and the excellent electron transfer properties of the reagents be exploited for a membrane-less configuration? Q3 How the temperature/pressure conditions affect the efficiency of the hydrogenation process? These questions were answered firstly by testing ECH with actual biocrude in a preparative H-cell at standard conditions and later by implementing it in a reactor at high temperature and pressure. In these latter conditions, at the anode we used actual PW from the HTL plant. Given the presence of organic and inorganic compounds, PW possesses quite high ionic conductivity, making it a good medium for water oxidation. Additionally, *in situ* ECH might have the beneficial side effect of performing electro-oxidation on the organic fraction present PW, as successfully achieved at ambient conditions in previous studies [30,31].

2. Materials and methods

Chemicals: Methanol (HPLC Plus, ≥99.9 %), ethanol (70.3 % v/v, TechnisSolv), ethanol (>99.5 %), sodium bicarbonate ($NaCO_3$, ReagentPlus®, ≥99.5 %, powder), sodium carbonate (Na_2CO_3, powder, ≥99.5 %, ACS reagent), and sodium chloride (NaCl, tested according to Ph. Eur.) were purchased from Sigma-Aldrich. Sodium Hydroxide (NaOH, pellets 98.5 %) was purchased by VWR. All reagents were used without further purification unless explicitly stated. All aqueous solutions used for electrochemical measurements were prepared with high purity de-ionized water obtained by passing distilled water through a nanopure Milli-Q water purification system (resistivity ~18 MΩ cm).

Nickel foam (>99.9 wt% purity) was purchased from MTI, Platinum mesh (>99.9 wt% purity) from Alfa Aesar, Titanium mesh (99.9 % trace metals basis) were purchased from Sigma Aldrich. Ion exchange membranes Nafion 117 (thickness 175 μm), Nafion Ionomeric hydroalcoholic solution (5 wt%), and anion exchange membranes Fumasep (FAA-3-PK-130) were purchased from Fuel Cell Store.

Biocrude and process water were collected during HTL of wheat straw (an abundant crop, largely used in straw-fired power plant in Europe and especially in Denmark [32]) at 350 °C at the continuous HTL pilot plant of Aarhus University [33].

BC was first pre-treated to remove any residual; this purification was done by rinsing intensively the BC with methanol at 60 °C. The composition of the used biocrude after purification is reported in Tables S1 and S2 in the Supporting Information.

Electrodes and membranes pre-treatment: Prior to its use, the Nickel foam was pre-treated to avoid the presence of impurities on its surface. The metal foam was rinsed intensively with isopropanol and successively with water before being immersed in a 2 M HCl aqueous solution for 5 min. The electrode was then sonicated in Milli-Q water for 10 min [34]. Before use, Nafion 117 membranes were pre-treated to remove any impurities and to fully convert to their H^+ form. The membranes were immersed 3 times for 1 h at 80 °C in 3 different solutions: H_2O_2 3 % in water, Milli-Q water, and finally in 0.5 M H_2SO_4 [35]. Before use, the membranes were rinsed with Milli-Q water until no more acid leaching was observed: *i.e.* the pH of the solution reached the base-line value of the Milli-Q water. In the case of Fumasep, the membranes were treated with 1 M KOH solution, for full conversion to their OH^- form, and kept in alkaline environment (NaOH 0.4 M).

Ambient pressure electrochemical characterization: Electrochemical Impedance Spectroscopy (EIS), and Chrono Amperometry (CA) were carried out by using CHI660E electrochemical workstation from CH Instruments. In all the three-electrode tests, Ni foam (geometrical active area 2 × 2 cm if not stated otherwise) was employed as working electrode (WE), a Pt mesh was used as the counter electrode (CE), and Ag/AgCl (leak-free electrode 1.6 mm OD, Alvatek Ltd. Cation) as reference electrode (RE).

CA experiments were carried out under a N_2 atmosphere in a two-compartment cell. The potential was set in the range of −1 V to −3 V vs Ag/AgCl and the experiment was left running up to 20 h. CA was carried out without IR compensation, due to the change (decrease) in resistance of the catholyte during the experiment driven by the cation electro-osmosis.

In typical CA experiments, the anolyte was a carbonate buffer pH 8–9, 1 M or 0.1 M, while the catholyte was a 40 mL solution of BC in MeOH (with a concentration 10 mg mL^{-1} unless otherwise stated). Representative values for the conductivity of the catholyte and anolyte solutions, were measured with a conductivity probe to be 50–60 $\mu S\ cm^{-1}$ and 75,000 $\mu S\ cm^{-1}$, respectively. Electrochemical blanks were performed in the same conditions as the CA experiments but at the open circuit potential thus without current circulating through the system; *i.e.*

WE, CE, and RE were present in the solutions.

High pressure electrochemical characterization: The electrochemical characterization of biocrude dissolved in methanol solution, was performed in a two-compartment glass cell (50 mL round bottom flasks) separated with either a single membrane (Nafion 117 or Fumasep), or a stack of one anionic (Fumasep) and one cationic membrane (Nafion 117). In this second case, the two membranes were sandwiched together and few drops of Nafion hydro-alcoholic solution were added to provide good ionic contact.

The working and reference electrodes were placed close together in the cathodic chamber, while the counter electrode was placed in the anodic one. In both the compartments magnetic stirrers were used. The temperature of the cell was regulated with an oil bath set at 60 °C. To allow for on-line data acquisition, the cathodic compartment was connected to an external circuit. The setup used (see Fig. S1a in the Supporting Information) allowed for monitoring the pressure increase as well as the local production of hydrogen in the cathodic compartment.

High pressure electrochemical characterization: A custom made set-up was designed and built to perform two-electrode membrane-less electrochemistry at high pressures (up to 200 bar) and high temperatures (up to 230 °C) (see Fig. S2 in the Supporting Information). A glass tube fitted with two electrodes (Nickel foam as WE, and Titanium mesh as CE both with a geometrical surface area of around 2 cm^2) was placed in the high-pressure reactor (HIP, United States) and used as electrochemical cell. The system was pressurized with nitrogen (grade 5, 99.999 % pure) at the working pressure and afterwards the reactor was heated to the working temperature by means on an aluminium heating block and 8 thermal resistances (total 2.5 kW). The electrochemical analysis was commenced once the biocrude oil migrated on the upper part of the cell (as seen from the polarization curves, see Fig. S3 in the Supporting Information) and lasted between 20 min and 2 h depending on the type of experiment performed. Afterwards, the system was cooled down to room temperature before depressurization to avoid boiling of the process water.

Thermal analysis: *Thermogravimetric Analysis (TGA):* Simple heating scan gravimetric measurements were performed with a TG 209 F1 Libra® vacuum-tight thermo-microbalance by Netzsch. Approximately 2 mg of sample were loaded into Al_2O_3 pans. A heating (N_2)-iso (N_2)-heating (air) method was used to determine the ash content of the BC residual. In this latter case, the samples were heated from 40 to 800 °C at a scan rate of 20 °C min^{-1}, afterwards the temperature was held at 800 °C for 4 h, and finally the temperature was increased to 1000 °C in air to burn the last carbonaceous residues.

Elemental analysis: The elemental composition of the samples was analysed using an Elementar vario MacroCube elemental analyser (Langenselbold, Germany). To quantify the presence of inorganic elements, biocrude oil samples were analysed via Inductively Coupled Plasma Optical Emission Spectrometry (ICP-OES) on an Optima 4300 DV (PerkinElmer, United States). Before ICP analysis, the samples were digested by acid-assisted microwave digestion (Multiwave 3000, Anton Paar, United States). Approximately 0.1 g of sample was added to a quartz digestion tube alongside 5 mL of nitric acid. The calibration curves were attained using standards from commercial certified solutions and by diluting the standards with nitric acid.

PW pristine samples and the samples after bulk electrolysis were analysed for the total organic carbon (TOC) by using a scalar FORMACSHT-I TOC/TN analyser.

IR spectroscopic analysis: *Fourier Transformed Infra-Red Spectroscopy (FT-IR):* The measurements on the solid residue of the sample were performed with a Nicolet iS5 FTIR-spectrometer equipped with iD5 ATR accessory (Thermo Fisher) and a Zinc Selenide crystal. The sample were analysed in the window from 400 to 4000 cm^{-1}, averaging 64 scans at a resolution of 1 cm^{-1}. Before FT-IR analysis, the samples were adjusted to match the pH (~6) of the pristine biocrude oil. The titration was performed using a 916 Ti-Touch by Metrohm. HCl (0.2 M) solution in methanol was used as titrant.

Chromatographic analysis: *Gas Chromatography-Mass Spectrometry (GC-MS):* Qualitative GC-MS analysis of bio-crude was performed on 10 mg mL^{-1} solution of biocrude in methanol with an internal standard (*p*-bromotoluene 20 μg mL^{-1}). Analysis was performed by using an Agilent 7890B GC coupled to a quadrupole mass filter MS (Agilent, 5977A). The GC injection port was operated at 100 °C in 1:1 split mode with the carrier gas, He, at 4 NmL min^{-1}, and the injection volume of 1 μL. The column was a VF-5 ms (60 m 0.25 mm, 5 m EZ-guard, Agilent) with a 5 % phenyl, 95 % dimethylpolysiloxane stationary phase. The column oven program started at 50 °C which was held for 2 min, progressing at 5 °C min^{-1} to 200 °C, at 20 °C min^{-1} to 320 °C (hold time 5 min) giving a total run time of 43 min.

GC-MS analysis of process water (PW) was performed with standard solutions prepared in chloroform. Aqueous phase (200 μL) was mixed with 5 w/w% sodium hydroxide solution (40 μL), and pyridine (40 μL). MCF (2 × 20 μL) was added, and the vial was vortexed for 30 s with each addition. Chloroform (400 μL) containing internal standard (4-bromotoluene) was added, and afterwards vortexed for 10 s. Sodium bicarbonate (50 mmol/L, 400 μL) was added, and the vial was vortexed for additional 10 s. The aqueous layer was removed, and the organic layer was transferred to a vial with insert [36].

The same GC-MS and column used for bio-crude analysis were used for PW analysis. The GC injection port was operated at 280 °C in 20:1 split mode with the carrier gas, helium, at 1 NmL min^{-1}, and the injection volume of 1 μl. The column oven program started at 60 °C which was held for 2 min, ramping at 5 °C min^{-1} to 200 °C, and at 20 °C min^{-1} to 320 °C (hold time 5 min), giving a total run time of 39 min.

In both cases ionization was performed by using an electron impact (EI) source in positive ion mode with electron energy of 70 eV. Data was acquired in scan mode (50–550 m/z). The MS was tuned using perfluorotributylamine. Data acquisition was performed using Masshunter.

Headspace Gas Chromatography (GC): The headspace gas concentration was measured with an Agilent 490 μGC. After injection, the gas was split in two lines each equipped with a column (10m MS5A column and 10m PPU PolarPlot) and a thermal conductivity detector (TCD). The MS5A column is capable of separating the permanent gases (O_2, N_2, CO, and H_2) while the PPU column was chosen for its ability to separate CO_2 from air, thus giving a quantitative value for the CO_2 concentration in the gas samples. Additionally the PPU column is also able to separate C_{2+} compounds which might be generated during electrolysis. The carrier gas used was He (grade 5, 99.999 %). The injection temperature was 110 °C and both columns were kept at 80 °C, while the pressure was increased from 50 kPa(g) to 150 kPa(g) during the first 30 s to obtain the best possible separation of the permanent gases and maintained constant until the end of the run (180 s). The columns were calibrated by using home-made mixtures containing 400 ppm of CO_2 in N_2 for the PPU and 2000 ppm O_2 in N_2 and a standard mixture (H_2 0.5 % ± 0.05 %, CO 4 % ± 0.4 %, CO_2 8 % ± 0.5 %, N_2 16 % ± 0.5 %, rest He, purchased from Air Liquide).

3. Results and discussion

3.1. Ambient pressure electrochemical tests

The purpose of the ambient tests was to investigate at lower scale ECH of biocrude; *i.e. i*) the effects of a direct electrochemistry on the H/C, O/C, and N/C ratios and *ii*) which families of compounds are affected by the electrochemistry. Direct hydrogenation of the BC was initially tested in a conventional H-cell with BC dissolved in methanol (10 mg mL^{-1}) while the anolyte was a 1 M sodium carbonate buffer at pH 9. Methanol was chosen as electrolyte for its known affinity with biocrude, being the solvent used for biocrude purification from the solid residues [37]. The typical electrochemical test was carried out by applying a negative potential at the Ni working electrode (between 1 and 3 V versus an Ag/AgCl reference electrode) at 60 °C (below the boiling temperature of methanol 64.7 °C at 1 atm) and for a run time up to 20 h.

For this exploratory work, we selected Nickel foam for its enhanced activity toward the key compounds constituting the biocrude in comparison with the parasitic hydrogen evolution reaction (HER) [18,38–40]. Previous work showed the efficiency of Ni together with Cu, and Ru towards the reduction of model compounds and bio-oils solved in electrolytic medium [38,41]. In this specific case, the electrode was tailored for a biocrude derived from wheat straw (WS) and thus towards the reduction of lignin and cellulose decomposition products (contain oxygenated aromatics, ketones, and furans [5,10,28]). Additionally, Ni and Ni-alloys are considered among the best materials to slow-down corrosion at HTL conditions. Here we notice that the H-cell experiments were not optimized for drawing the highest possible currents, which were limited by *i*) the conductivity of the catholyte solution, ultimately determined by the solubility of BC in methanol at the temperature used in the experiments; and *ii)* possible mass transfer limitations.

Due to the nature of the buffer solution used as anolyte, the separators must possess a quite significant resistance to the cation electromigration. This is needed to avoid the shuttling of Na^+ from the anolyte to the catholyte under an applied electrical field, which ultimately reduces the flux of protons and thus it represents a source of energy dissipation. Therefore, the separators used were either anion exchange membranes (AEM, Fumasep) or a combination of a cation exchange membrane (CEM, Nafion 117) and one AEM bonded together with Nafion solution (in the following referred to as bipolar membrane, BPM). At the relatively large ionic strength (1 M) of the anolyte solution, AEM membranes became partially permeable to the cations (mostly Na^+ ions) due to the reduced Debye screening length inside the ionic channel network [42]. The reduced ion permselectivity resulted in cation (mostly Na^+ and K^+ ions) crossover towards the catholyte, which represents an energy penalty for the electrochemical system. The non-ideal cation permselectivity can be seen for both the AEM and BPM configurations as cation cross-over, measured via ICP-OES. The concentration of Na^+ and K^+ in the catholyte after bulk electrolysis is reported in Table S3 in the Supporting Information, for both AEM and BPM configurations and contrasted with the ion content in electrochemical blanks. As reference, Table S3 also includes experiments with a CEM membrane. Due to the buffer solution used as anolyte, the mobile cations are mostly H^+ and sodium cations. The Na^+ content in the electrochemical blanks is an indication of the ion diffusion only due to the difference in Na^+ concentration in the anolyte and catholyte solutions. As clearly shown in Table S3, the Na^+ for both AEM and BPM blanks was quite similar and around 2 mM. This is the result of the non-ideal permselectivity of these membranes at high ion concentration. However, both configurations were quite effective when compared to the reference blank with a CEM.

Interestingly, by using BPM the Na^+ crossover during bulk electrolysis was significantly reduced with respect of AEM. This was possibly due to the larger ionic resistance provided by the BPM. In these conditions after 20 h of electrolysis the Na^+ concentration was only 3.7 mM

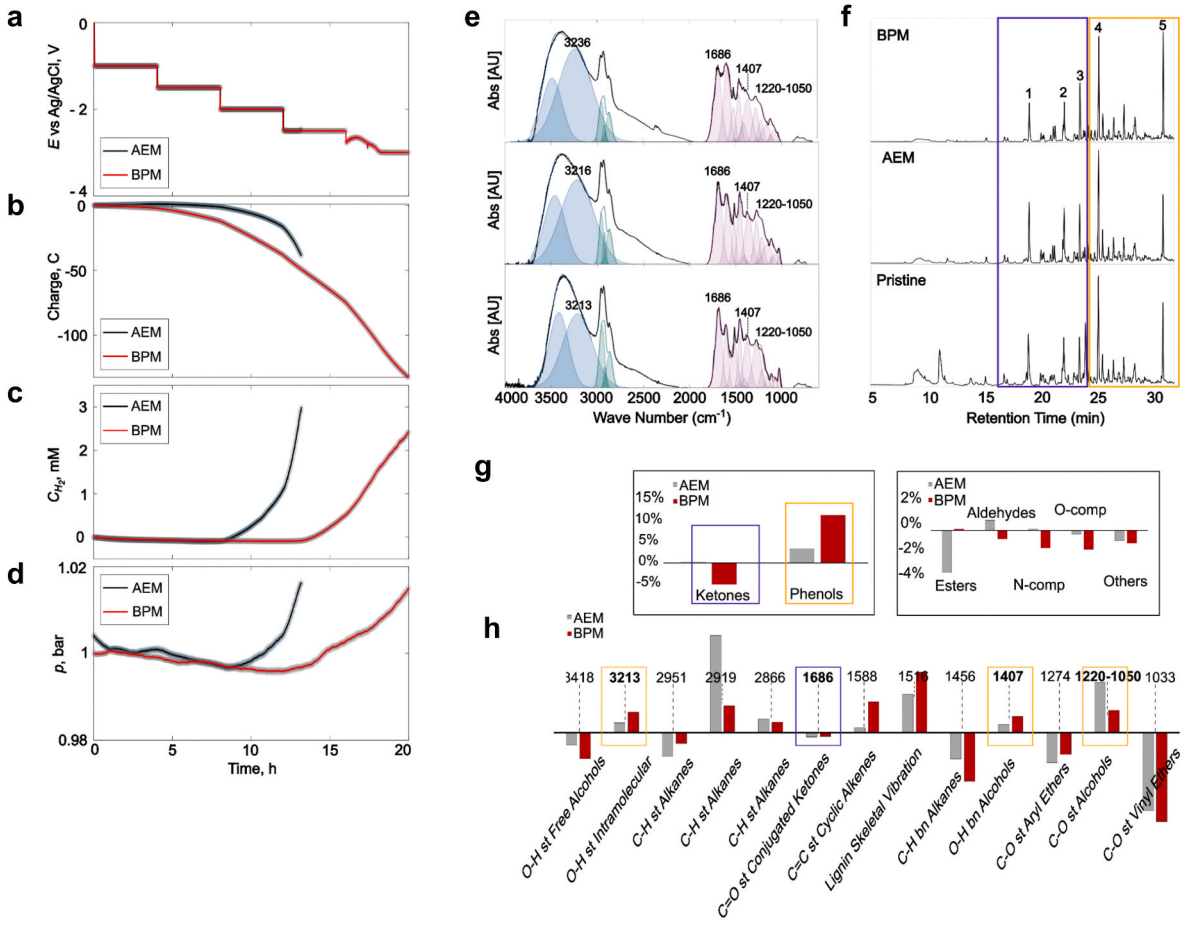

Fig. 1. a–d Electrochemical tests of biocrude with anion exchange (AEM, black symbols) and bipolar membranes (BPM, red symbols): Time evolution of **a** half-cell voltage cathodic side, versus Ag/AgCl reference electrode; **b** calculated flow of charge from the time-integration of the current circulating in the system; **c** local H_2 concentration measured from an H_2 micro-sensor placed over the gas-liquid meniscus in the catholyte compartment: and **d** total pressure at the cathodic compartment. **e–h** FT-IR and GC-MS analysis: **e** Deconvolution of IR spectra: The pH of solutions was lowered to ~6, to match the pH of the pristine biocrude, by titration with 0.5 M HCl in MeOH; **f** GC chromatograms of the oil phase: peak attribution is reported in Table S5 in the Supporting Information. Comparison of the families of compounds with increasing or decreasing concentration after electrolysis with respect to the pristine biocrude: **g** from GC-MS and **h** from IR analysis. For all tests: Catholyte BC dissolved in methanol (10 mg mL^{-1}); anolyte 1 M sodium carbonate buffer at pH ~9.

(against 2.1 of the electrochemical blank and 8.1 mM of the AEM configuration).

From the Na^+ concentration and by considering the volumes of the electrolyte solution at the end of the experiments, we calculated the charge dissipated in the ion transport. For the BPM configuration the increase in Na^+ concentration corresponds to around 2 C of charge used to transfer Na^+ between compartments (compared to the total charge of 133 C). In other words, only around 1.5 % of the charge provided to system was dissipated on transporting Na^+ ions. This must be contrasted to the AEM membrane where around 20 % (around 10 C) of the charge was dissipated on the ion transfer alone. Similar results were found by using thermal gravimetric analysis, where lower ash contents (around 4.5 %) were found by adopting the BPM configuration (see Fig. S4 in the Supporting Information). Due to the high energy penalties resulted from the ion cross-over with CEM and AEM, in the following we will focus our discussion on the results obtained for the BPM configuration, comparing the results with the AEM only when needed for the sake of explanation.

Fig. 1a–d show a comparison between the results of a bulk electrolysis performed with AEM and BPM configurations, as a step voltammetry (electrical potential bias between −1 and −3 V vs Ag/AgCl, steps of 0.5 V of duration of 4 h). Fig. 1a–d report the time evolution of the potential bias at the cathode (versus reference Ag/AgCl electrode), transferred charge, the local hydrogen concentration, and the total pressure of the system, respectively. The tests were carried out until the total pressure of at the cathode reached around 1.015 bar (Fig. 1d). Fig. 1b shows that a significantly higher charge was transferred when using the BPM configuration, since the onset of the pressure increase was significantly delayed with respect to the AEM configuration.

We hypothesize several different electrochemical reactions that can happen at the cathode: these include possible hydrogenation of the biocrude, electrochemical cleavage or splitting of high molecular weight molecules, as well as hydrogen evolution reaction (HER). To check the possible competitive HER reaction happening at the cathode, we placed a hydrogen micro-sensor just above the meniscus of the liquid (see Fig. S1a). While the absolute value of the H_2 concentration measured by the micro-sensor (see Fig. 1c), could not be used for quantitative calculations of the production of H_2 due to the local nature of the measurement, it still provided a precise indication of the onset of the H_2 production. HER was probably associated with the water splitting at the cathode. Indeed, water could be exchanged between the compartments via the mechanisms of: (*i*) diffusion, generated by the concentration difference, and (*ii*) electro-osmosis being water transported as hydration shell of the ions electro-migrating from the anolyte to the catholyte compartments when an electrical potential difference is applied to the system. Additionally, the methanol could itself contain a small percentage of water as impurity. A blank test, pure methanol (containing lithium tetrafluoroborate, to match the initial conductivity of the BC in MeOH) was performed to check such a hypothesis. The results confirmed that the HER was still present; however, in this latter case the onset of the hydrogen production coincided with the onset of the charge, and no other products different from H_2 were detected by GC. This indirectly confirms that no electrochemical reactions involving methanol were present at the potential differences invesitgated in this work.

From the comparison in Fig. 1c, we can infer that the BPM configuration allowed for a significant delay in the hydrogen production with respect to the AEM. For AEM, only 1.5 C of charge (see Table S4 in the Supporting Information) were delivered before the onset of the hydrogen production, while in the former case (BPM) the charge provided to the system was around 52 C, a factor 10 times higher. Here it is worth noticing that the results discussed above regarding the charge dissipated for ion migration, suggest that also after the onset of the H_2 production, HER cannot be the only reaction happening at the cathode. With reference to the results for the AEM configuration, if the HER were the only contribution to the charge transferred in the system, then the onset would have been after providing around 10 C: *i.e.* the charge calculated for the Na^+ transport. Therefore, the data of the charge before the onset cannot be straightforwardly used to calculate how much charge was used to promote reactions different from HER. To this end, a better estimation of the cumulative hydrogen production can derive from the analysis of the pressure profiles (Fig. 1d). The pressure showed a significant increase after approximately the same time as the onset found in the hydrogen concentration. In this case, the first decreasing segment of the curve was due to the decrease in temperature of the reservoir during the duration of the experiment, which in turn lowered the partial pressure of methanol. The temperature decrease was just due to the nychthemeral cycle. The amount of charge used for H_2 production in the two cases can be assessed if we assume that the increase in the total pressure was only due to hydrogen formation: *i.e.* no other reaction generates products in the gas phase. This assumption seems plausible since from the analysis of the gas space we did not identify any other compounds except H_2 and CO_2. From the measured pressure increase and by using the ideal gas law and Antoine equation for the liquid-vapour equilibrium of methanol, we calculated approximately 38 C of charge dissipated to produce hydrogen with AEM configuration, while 55 C with the BPM. The difference was due to the different temperatures of the expansion vessel at the beginning and the end of the experiment.

The figures estimated for the charge dissipated for the ion transport as well as for the hydrogen production, should be considered only indicative, and prone to systematic errors in the measurements. Indeed, for the AEM configuration, the balance between the measured charge delivered to the system and the ones calculated from ion transport and H_2 production does not close (overestimation of ~20 %). On the other hand, they clearly show that a significant part of the charge was available for electrochemical reaction other than HER for the BPM configuration, while nil or, at the most, minimum electrochemical work different from HER was performed in the AEM configuration.

Next, we performed elemental analysis on the residue after bulk electrolysis and complete evaporation of the methanol phase. The results were compared with the pristine biocrude (see Table 1). The samples for the elemental analysis (including pristine BC) were dried at the same temperature of the experiments to avoid the evaporation of any volatile compounds potentially produced during electrolysis. Here we note that the pristine BC, had somehow a lower H content compared to similar oils produced from HTL from wheat straw [33], and this can be possibly associated to our methodology used for its purification (extensive rinsing the BC with methanol at 60 °C) or the way the BC was stored.

For the BPM configuration, the elemental analysis after bulk electrolysis indicates a decrease in carbon and sulphur content, similar value for nitrogen, and a slight increase of the hydrogen content with respect to the pristine biocrude (see Table 1, concentrations reported as weight %). The sulphur concentration was close to the detection limit of the instrument used, and no definitive information can be drawn for this compound. The oxygen content (reported without standard deviations) was calculated as mass balance of the detectable compounds and ashes, and, as such, it is the figure most prone to errors. The oxygen content for the AEM configuration was similar to the one of the pristine BC, while for the BPM configuration a higher value was calculated. This is the results of the low value for the ashes found in the TGA. The weight concentrations are influenced by the amount of ashes present in the sample, and a better comparison can be drawn by considering the atomic ratio of hydrogen, nitrogen, and oxygen over carbon (last three columns in Table 1). These atomic ratios show that the relative amount of nitrogen is quite constant while the H/C ratio increases after electrolysis. It is also possible to notice that the value for the O/C ratio are the most scattered, because are influenced both by errors in the mass balance and uncertainties on the ashes content. Similar consideration can be made for the AEM configuration, even if the effects of the electrolysis are much less pronounced. These results suggest that an increase in the hydrogen content of the biocrude via direct electrochemical hydrogenation route is indeed possible.

Afterwards we investigated which families of compounds were

Table 1
Elemental analysis of the biocrude pristine and electrochemically treated at ambient pressure and 60 °C and in conditions similar to HTL plants.

	Charge (C)	Weight %						Atomic ratios without ashes		
		C	H	N	S	O	Ash	H/C	O/C	N/C
Pristine	0	72.9 ± 0.54	6.44 ± 0.06	1.29 ± 0.01	0.11 ± 0.003	17.4	2.2 ± 1.0	1.06	0.18	0.015
Ambient pressure tests										
AEM	40	65.35 ± 0.41	6.08 ± 0.14	1.1 ± 0.01	0.4 ± 0.02	18.1	11.2 ± 0.8	1.12	0.18	0.014
BPM	133	65.18 ± 0.93	6.51 ± 0.32	1.1 ± 0.01	0.1 ± 0.01	23.7	4.5 ± 1.5	1.2	0.26	0.015
High pressure tests										
Blank 150 °C	0	70.8 ± 0.14	8.2 ± 0.30	1.2 ± 0.01	0.1 ± 0.03	17.1	3.1 ± 0.5	1.39	0.18	0.015
10 V 150 °C	75	68.3 ± 0.20	9.3 ± 0.42	1.1 ± 0.01	0.1 ± 0.01	17.8	4.1 ± 0.6	1.63	0.19	0.014
20 V 150 °C	102	68.4 ± 0.59	7.8 ± 0.56	1.1 ± 0.02	0.1 ± 0.01	18.8	4.7 ± 0.8	1.37	0.2	0.014
30 V 150 °C	195	67.8 ± 1.37	7.2 ± 0.36	1.1 ± 0.1	0.1 ± 0.01	19.2	5.7 ± 0.8	1.27	0.2	0.014
Blank 200 °C	0	70.7 ± 0.48	7.9 ± 0.14	1.2 ± 0.02	0.1 ± 0.01	16.8	4.0 ± 0.4	1.34	0.17	0.015
10 V 200 °C	175	68.6 ± 0.36	8.9 ± 0.25	1.2 ± 0.01	0.1 ± 0.01	15.4	6.9 ± 0.3	1.56	0.15	0.015
20 V 200 °C	74	74.1 ± 3.17	7.0 ± 0.10	1.3 ± 0.01	0.1 ± 0.01	13.8	4.3 ± 0.4	1.13	0.14	0.015
30 V 200 °C	420	64.4 ± 1.00	6.7 ± 0.28	1.1 ± 0.01	0.1 ± 0.01	17.8	12.0 ± 3.8	1.24	0.18	0.015

possibly involved on the hydrogenation reactions. We focused our attention to the hydrogenation of aromatic rings [24,43], phenols, and the reduction of carbonyl groups (*e.g.* ketones and aldehydes) [22] since they were previously achieved for model compounds. To this end, we carried out both FTIR spectroscopy and GC-MS on samples after methanol extraction.

At the onset, we acknowledge that BCs are extremely complex mixtures of compounds that cannot be fully identified via an analytical method. Thus, IR and GC-MS analysis can give only a (very) partial view of the BC composition, and their figures must be used only to highlight general trends. In general, the quantified fraction of bio-crude (relative to its mass) by GC-MS is very low. For instance, performing data analysis on ref. [30], one can notice that only around 3.3 wt% and 1.7 wt% of the BC has been quantified for bio-crudes derived from HTL of miscanthus and willow respectively (both lignocellulosic biomass as in this work). Taking into account these shortcomings, the results of both FTIR and GC-MS indicate an increased number of phenols after electrochemical treatment, probably due to the cleavage of aryl ether bond of lignin-derived compounds, observed previously in the alkaline or thermal hydrolysis of lignin [44,45]. For this discussion, we refer to lignin-derived as the lower molecular weight compounds produced from lignin during the HTL process. Indeed, lignin, cellulose etc. have been decomposed (de-polymerized) during HTL to *e.g.* oxygenated aromatics, light oxygenates, and sugars. The IR spectra of the biocrude after electrolysis (see Fig. 1e and h) show an increase of the absorption peaks typical of alcohols and phenols (see Table S5 in the Supporting Information for the IR peak assignment). More specifically, the band 3418 cm^{-1} was attributed to the O–H stretching of free water, acids and alcohols and the one at 3213 cm^{-1} to the intramolecular O–H stretching of alcohols [45]. As expected, the peaks between 1407 and 1361 cm^{-1} and 1217–1071 cm^{-1} associated with the C–O bending and stretching of primary, secondary, and tertiary alcohols increased as well after electrolysis [46,47]. Both the bands at 1588 and 1516 cm^{-1}, associated to C═C stretching of alkenes and aromatic back bones stretching [47], increased after electrolysis. The increase of signals of aromatic ring stretching (1516 cm^{-1}) matches well with the higher concentrations of free phenols derived from the oligomers from lignin [48].

The bands between 2950 and 2860 cm^{-1} were attributed to symmetrical and asymmetrical C–H stretching of methyl and methylene groups. We observed a change of intensity of the three peaks belonging to these groups after the electrolysis [45]. Peaks attributed to conjugated ketones can be observed at 1686 cm^{-1} [47] and their presence decreased after electrolysis. Finally, the bending of methylene groups of alkanes and aromatics (1456 cm^{-1}) [45] decreased as well as the C–O stretching and bending of ethers (1274 and 1033 cm^{-1} respectively). This latter band, commonly associated with the aromatic ether C–O–C bond of lignin showed a decrease as expected [44].

The chromatograms obtained by GC-MS (Fig. 1f and g) indicate the same trend already observed and commented for the FTIR: an increase in the signal of phenols probably due to the cleavage of aryl-ether lignin-derived bonds. The compounds containing nitrogen were not modified by the electrochemical treatment and their amount was constant around the 17 % compared with the pristine BC. This result corroborates the measurements for N content from elemental analysis. Similarly, the other minor components of the oil, as furans, aldehydes, and carboxylic acids with amounts of 4 %, 0.6 % and 2 %, respectively were not modified by the electrochemistry. Other components as linear and aromatic hydrocarbons decreased slightly after electrolysis. Ketones, whose major components are cyclopentenones decreased from 43 % to 35 % (AEM) and 29 % (BPM). On the contrary, phenols increased from 17 % to 28 % (AEM) and 37 % (BPM). Higher molecular weight compounds as long chain derived from lignin or cellulose present in the mixture were not detected by the GC-MS due to the limited temperature at which the instrument works (300 °C), thus not allowing the vaporization of high boiling point components.

The results from thermogravimetric analysis (see Fig. S4 in the Supporting Information) show that the biocrude treated with BPM had a larger weight loss between 40 °C and 300 °C with respect to the pristine biocrude possibly associated to the presence of more volatile fractions derived from the decomposition of oligomers of the lignin producing phenols having $T_b = 230 - 270$ °C (refer to Table S6 in the Supporting Information for the boiling points of the fractions identified from GC-MS analysis). On the other hand, the electrochemically treated sample showed lower mass change in the range between 300 °C and 800 °C compared to the pristine biocrude. The species decomposing at this range of temperatures were not detected by the GC-MS and can be associated with polymeric structures derived from lignin or others high molecular weight compounds. The remaining ashes were negligible.

The analysis of the ambient pressure electrochemical tests indicates that the biocrude can be electrochemically upgraded, at least in terms of hydrogen content. To further prove this point and to test the possibility of performing the oxidation reaction with process water, we designed an additional experiment. Here we employed the best configuration used for the ambient pressure tests (BPM), methanol/BC at the cathode, and process water at the anode. We report the results in Fig. S5 in terms of the gas evolution in the anodic and cathodic chambers. The main point is the presence of a region of voltage where we observed an evolution of CO_2 in the cathodic compartment, possibly associated O heteroatom removal from oxygenated compounds. As discussed above, this reaction is in competition with HER, which started to evolve when the cathode is biased at −2.5 V. Interestingly, there was an evolution of CO_2 also in the anodic chamber, which is likely associated with the oxidation of organic compounds present in the PW.

3.2. High pressure electrochemical tests

Next, we considered an electrochemical process at similar conditions of the HTL, to assess the feasibility on an *in-situ* upgrading after the HTL reactor in the cooling down section of the process. Here we aimed at confirming the preliminary results obtained at the ambient pressure, at conditions relevant for the industry and thus deliver a *proof-of-concept* of the reactor. To the best of our knowledge, electrochemistry of BC at high temperature and pressure was not reported before in the open literature. These experiments presented several challenges: the most notable are *i*) the design of the system, *ii*) the choice of materials and catalysts for the high-temperature and high-pressure conditions and *iii*) possible re-oxidation of electrochemically hydrogenated BC, either by the O_2 initially present in the reactor or the one produced during bulk electrolysis. The chosen configuration and materials immediately follow.

High-pressure tests were conducted in the reactor described in the Supporting Information (Fig. S2 in the Supporting Information) at pressure up to 100 bar and temperature of 150 °C and 200 °C. The pressure of the system at the test conditions, was determined by the initial N_2 pressure (reactor filled at around 50 bar with grade 5 N_2 at room temperature), its expansion and the partial pressure of water at the test temperature. We limited the pressure of the experiments to around 100 bar for safety reasons. The choice of the temperature at which perform electrochemistry in an HTL plant, is somehow flexible. An HTL plant is optimized to obtain the maximum heat recovery to reduce operational costs: A cascade of heat exchangers is therefore implemented to transfer heat from the outlet stream (BC and process water) to the inlet stream of wet biomass. Therefore, the possible electrochemistry on the BC and process water can be performed at any temperature ranging from the outlet temperature of the reactor (up to 350 °C) to, theoretically, room temperature. The temperature lower bound of our experiments, was selected according to preliminary tests showing an inversion of the position of the biocrude and PW phases (see Fig. S3 in the Supporting Information) when the reactor reached a critical temperature. Below this critical temperature, the biocrude was positioned at the bottom of the cell, due to its high viscosity. However, when the temperature of the system increased, the viscosity of the biocrude was significantly lowered and an inversion of the two liquid phases, driven by the density difference, begun. Experimentally, we have observed the starting point of the phase inversion around 75 °C, being 150 °C the lowest temperature where we could clearly electrochemically measure it. On the other hand, the temperature upper bound was chosen safely below the temperature-pressure rating of the lead wires fitting (max 232 °C).

The electrochemical tests were carried out in a membrane-less configuration leveraging on the immiscibility of the two phases. The electrodes were spaced 5–10 mm apart to ensure that the interface of the BC-PW would comfortably be between them during the duration of the experiments. A relatively precise knowledge of the position of such an interface would be needed to deploy and optimize high pressure ECH in the cascade of the heat exchangers.

For these tests we investigated similar conditions to the HTL also in terms of the composition of the two phases. More specifically, biocrude was used as catholyte and process water as anolyte. Nickel foam and titanium meshes were used as cathodes and anodes, respectively. Both Ni and Ti (in the oxidised form at test conditions) are distant from the vertices of their respective volcano plots for the hydrogen and oxygen evolution reaction, respectively [49]. Therefore, they might promote other electrochemical paths different from HER and OER. Ni is normally employed for H_2 production in alkaline electrolysis, however to boost its efficiency extremely alkaline solutions are adopted. Moreover, Nickel and high Ni content alloys (*e.g.* Inconel) are among the preferred materials for the HTL reactor and piping, because of their proved resistance towards corrosion at the HTL process conditions [50]. Ti was chosen instead of Ni at the anode due to the higher resistance [51] in acidic solutions (PW has pH ∼ 4 at room conditions). PW contained a large amount of organic compounds (see Table S2 Supporting Information) hence ensured a quite significant ionic conductivity (∼14 mS cm^{-1} at room temperature). Typical electrolysis were carried out for 20 min, to approach the typical residence time of an HTL plant [52]. Indeed while inside the HTL reactor the normal residence times are of the order of 20 min, in the following cascade of heat exchangers these values drop to around 5 min.

At the temperatures investigated in the present work, biocrude was prone to oxidation also when modest O_2 concentrations were present in the gas phase. After preliminary tests at different O_2 concentration inside the reactor, we selected an initial O_2 concentration between 200 and 400 ppm, to minimize the effects of thermal oxidation, still keeping the oxidation agent to mimic real operative conditions. To the best of our knowledge, there are no information in the open literature regarding the O_2 level inside a continuous HTL plant. In an actual plant, the concentration of O_2 is maintained at minimum level given the fact that the biomass and water are pressurized into a long tubular reactor as described in Ref. [6] However, low levels of oxygen, originating from atmospheric air but also from the dissolved oxygen present in the biomass/water slurry, enter the system through the continuous high pressure pumping of the feed slurry.

Examples of electrolysis performed at 150 °C and 200 °C are reported in Fig. 2 a–d, while Fig. 2e and f show the time evolution of the current density (in mA cm^{-2}, scaled over the geometrical surface area of the catalysts) and the calculated charge (in C) at different values of the applied potential difference. From Fig. 2b is clear that a significant positive effect of the temperature can be seen both at the beginning of the experiment (limit of no mass transfer limitation) and as terminal current.

After a time-lag period (shown as dashed curves in Fig. 2e) lasting from approximately 50 to 200 s, the current circulating in the system decreased over time; this feature seemed more marked for the tests conducted at high electrical potential difference. Afterwards, and within the duration of the experiment, the current approached an approximately stable value. Since the electrochemical reactor was not equipped with any active stirring, the fluid mixing was essentially due to natural convective streams inside the cell. Therefore, significant mass transfer limitations due to ion diffusion were expected. This can explain the decrease of current during the experiment and its approach to a terminal current significantly below the maximum. In any case, it is evident that larger current and charge were delivered to the system with respect to the batch tests performed at low temperature and ambient pressure (for the current typically 50 to 100 times higher). These latter figures were calculated considering the terminal current, and therefore are conservative values. Here we notice that if the concept of direct electrochemical hydrogenation were to be used in a real continuous HTL system, these mass transfer limitations would be greatly mitigated due to the flow (forced convection) of the produced biocrude. Fig. 2f shows that the charge increased by increasing the applied potential. The delivered charge was influenced by the total resistance of the electrochemical cell, mostly originating from slight differences in the electrode positioning inside the reactor. The total cell resistance was monitored before and after bulk electrolysis with electrochemical impedance spectroscopy (EIS, see Figs. S6 and S7 in the Supporting Information). Before electrolysis the total resistance of the cell (real part of the impedance at low frequency) was between 100 and 400 Ω. From the analysis of the EIS data before electrolysis a conservative value for the ion conductivity (see Fig. S8 in the Supporting Information) at high-pressure high-temperature conditions could be estimated to be 2400 μS cm^{-1} and 4700 μS cm^{-1} at 150 °C and 200 °C, respectively. After electrolysis the cell resistances were larger (up to 1000 Ω) and the distinction between the charge transfer resistances of anolyte and catholyte more visible. This latter phenomenon can be an indication that the two phases after electrolysis were better separated. The main point from the EIS results is that the distinction of the two phases is quite evident, thus the immiscibility of the water and oil phases was preserved

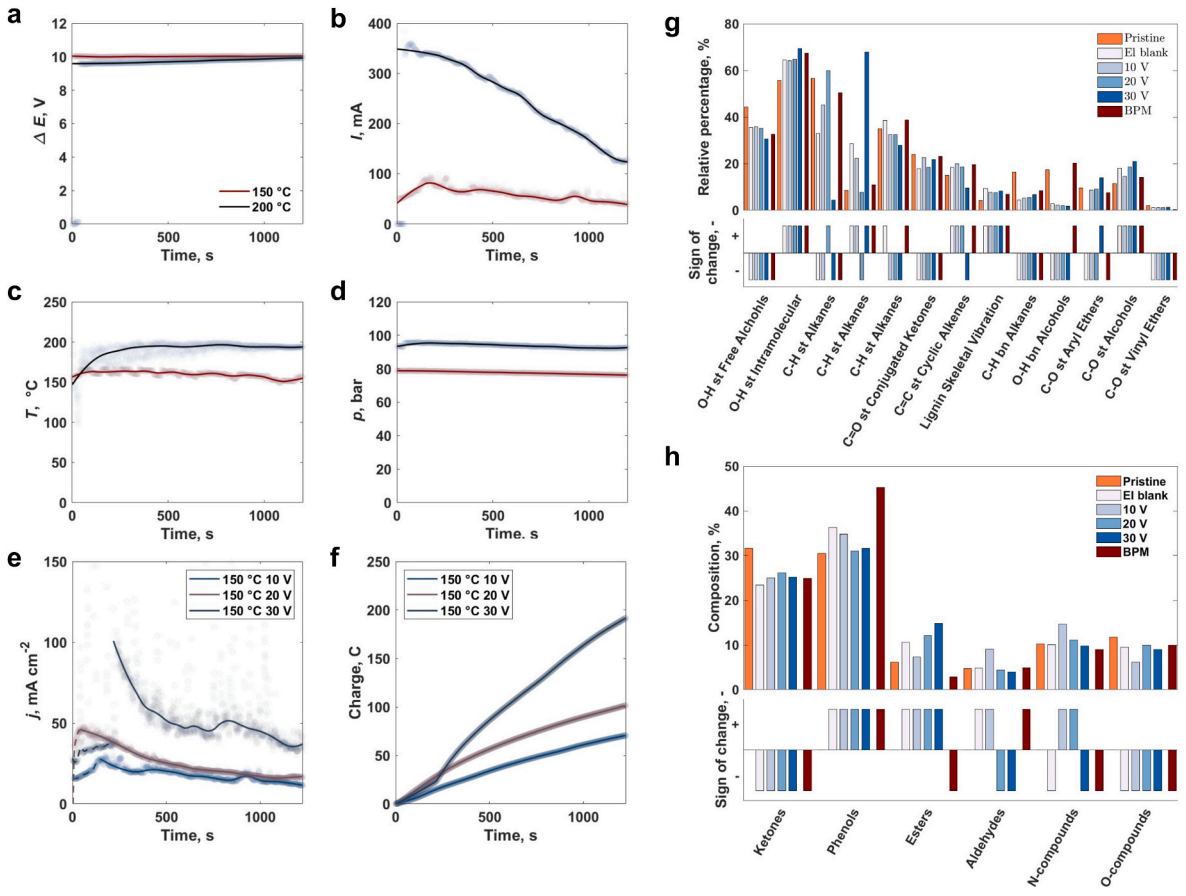

Fig. 2. **a–d** Electrolysis performed with biocrude and process water at 150 °C (red colour) and 200 °C (blue colour). Symbols represent raw experimental data and the continuous curves are smoothed values to guide the eyes **a** applied potential difference at the electrodes; **b** electrical current circulating in the system; **c** temperature; and **d** total pressure of the system. **e** Current and **f** charge of the potentiostatic analysis performed at 150 °C, with applied potentials of 10 V, 20 V and 30 V for 20 min **g** upper panel: Relative percentage of the bands deconvoluted from the FTIR spectra (reported in Fig. S9 in the Supporting Information) of the pristine, electrochemical blank, and samples treated at 10 V, 20 V and 30 V at 150 °C. Lower panel: sign of the change with respect to the pristine BC. **h** Upper panel: Composition of detectable compounds in GC-MS of the biocrude electrochemically treated of the pristine, electrochemical blank, and samples treated at 10 V, 20 V and 30 V at 150 °C. Lower panel: sign of the change with respect to the pristine BC. In **g** and **h** the results for the BPM configuration at ambient pressure and 60 °C (dark red) are added for the sake of comparison.
Conditions, biocrude 1–1.2 g, process water 3–3.5 mL; Ti (anode), Ni (cathode).

also in HTL conditions, which allowed us to perform electrolysis tests in a membrane-less configuration.

Elemental analysis was performed in the samples extracted after bulk electrolysis as well in electrochemical blanks (reported in Table 1). These latter tests were performed at the same temperature, O_2 concentration, and the same amount of time (including heating and cooling down of the reactor) as the bulk electrolysis. In Table 1 we report the concentration (for C, H, N, and S in terms of weight %) also with respect to the electrochemical blanks since the H content in these latter tests was higher with respect to the pristine biocrude. Therefore, a direct comparison of the H composition with the pristine biocrude could result in an overestimation of the effect of electrolysis at high pressure and temperatures.

Table 1 shows that only the tests performed at the lower applied voltage (10 V of total cell potential at both 150 °C and 200 °C) resulted in a clear increase in the H/C atomic ratio, while the O/C ratio was substantially unchanged. Here we stress again that while the O concentration is calculated from the mass balance hence prone to systematic error, while the O/C ratio is also affected by experimental uncertainties on the ash content from TGA measurement. In the other experiments, even though a larger amount of charge was transferred to the electrochemical cell, a lower H/C ratio was measured with respect to the electrochemical blanks. We have ascribed this phenomenon to an *in situ* re-oxidation of the biocrude (which could have been partially reduced via electrochemistry) due to the flux of pure oxygen generated in the anodic compartment. Indeed GC-MS data on the process water indicates that the composition of the detectable organics compounds in the PW was substantially unchanged after bulk electrolysis, however we found a marked decrease in TOC (see discussion below). Therefore, we hypothesize that albeit part of the produced O_2 was consumed oxidizing the organic compounds in the PW, a significant fraction was still available to migrate to the oil phase for re-oxidation of the BC.

To be able to understand better ECH, we performed FTIR and GC-MS measurements on both the biocrude and process water phases. FTIR (Fig. 2g and Figs. S9–S11 in the Supporting Information) and GC-MS analysis (Fig. 2h and Figs. S12 and S13 in the Supporting Information) confirmed the trends found in the experiments carried out at ambient pressure. The main results of the FTIR deconvolution are reported in Fig. 2g, which shows the difference in the peak area of the electrochemically treated biocrude at 150 °C referred to the pristine biocrude. Fig. 2h reports the composition of the detected compounds via GC-MS of the biocrude electrochemically treated, the pristine, the electrochemical blank, and the samples electrochemically treated at 150 °C. The full set of results, including the experiments carried out at 200 °C can be found in the Supporting Information. For the sake of comparison, Fig. 2g and h contrast the results of high-pressure electrochemistry with the one obtained for the most performant H-cell configuration (with bipolar membranes and referred to the pristine biocrude). The same arguments

discussed in the section of the results of the electrochemistry at ambient pressure can be used here. The concentration of ketones and oxygen-containing compounds decreased. The main difference lies on the O–H peaks, possibly associated to the phenols, which composition decreases in all the high temperature tests (including the electrochemical blanks). Here we note however that a significant increase of the phenol content was observed in the GC-MS analysis of the process water (see discussion below and Fig. S16 in the Supporting Information). We attributed the decrease of O–H concentration during high temperature experiments to the migration of the phenols compounds to the process water, driven by their solubility.

TGA results indicate (see Fig. S14 in the Supporting Information) that the biocrude electrochemically treated at 150 °C had similar ash content with respect to the respective electrochemical blank. Additionally these electrochemical conditions result in a slightly better performance, given the higher mass loss in the temperature range 0–800 °C (see TGA and DTG results in Figs. S14a and b in the Supporting Information, respectively). This indicates a larger concentration of volatile fractions. The mass loss up to 80 °C was attributed to the family of cyclic ketones while the one around 250 °C can be attributed to evaporation of phenols (boiling point between 230 and 270 °C). Different results have been obtained for the tests where higher charge was delivered to the system. In this case the weight loss is lower than the electrochemical blanks; we associated these experimental observations to the possible re-oxidation of the biocrude from the O_2 generated in the anolyte. These findings are in line with what observed from elemental analysis. The characterization of the electrochemically treated biocrude suggests that a direct partial hydrogenation of the biocrude can be achieved at HTL conditions. However it also indicates that at the working conditions of an HTL plant, the process conditions in terms of temperature, oxygen concentration, and electrical potential difference must be specifically tailored to avoid BC re-oxidation.

Finally we analysed the effects of conducting electrolysis at high pressure and temperature on the PW phase. First we conducted experiments to assess the extent of the wet oxidation; *i.e.* oxidation of the organic compounds present in the PW due to the O_2 present in the head space. We performed wet oxidation experiments at two different levels of initial O_2 concentration (see Fig. S15 in the Supporting Information). The results show that at the initial O_2 concentration chosen in this work (100–400 ppm) the purely thermal effect of the wet oxidation was minimal, hence this phenomenon did not alter substantially the electrochemical results. GC-MS analysis of the process water shows an increase in the phenols content (see Fig. S16 and Table S9 in the Supporting Information) compatible with the migration of this fraction from the BC to the PW during electrolysis. The composition of the other detectable compounds did not differ substantially between the sample from bulk electrolysis and blanks. On the other hand, the TOC analysis performed on PW after electrolysis (Table S10 in the Supporting Information) showed a significant decrease on the total carbon (up to 30 %). This is associated to the oxidation of the carbonaceous compounds driven either by the oxygen produced in the aqueous phase, or from direct electrochemical oxidation. These results are also compatible with the ambient pressure tests performed with methanol/BC and process water (reported in Fig. 5 of the Supporting Information).

The reduction in TOC can be associated to the decarboxylation reaction at the anode side. Here we note that these reactions have little to no influence in the C and H content in the BC phase. Indeed, the concentration of organics present in the PW (see Table S10 in the Supporting Information) is around 10–20 g/L which scaled by the volume of PW in the reactor (3 mL) and an average molecular weight will give a total 1–2 mg. This amount would not suffice to change in any measurable way the C and H content of the BC (around 1g). Indeed, this would be equal to a change of maximum 2/1000 in the BC phase weight. This would be the case when we assume the best-case scenario when these hypotheses are fulfilled: 1) all the organics are converted, which would entail a perfectly clean water that we do not experimentally observe; 2) the H/C ratio of the products at the anode had an average ratio above 1.4; 3) the affinity of such products is higher for the BC than PW. We therefore believe that the observed changes in the BC C and H contents are due to the direct hydrogenation and not from the decarboxylation reactions at the anode side because the effect is negligible (max 0.1 %).

Finally, the reduction in TOC for the PW represents a beneficial side effect of the proposed electrochemical method, since for some specific types of biomass (*e.g.* sewage sludge from waste water treatment plants) the PW cannot be recirculated in the system and needs to be purified before its disposal [53].

4. Conclusions

In this work we demonstrated a *proof-of-concept* of a direct electrochemical approach to hydrogenate the biocrude oil produced from HTL. We demonstrated the electrolysis in conditions close to the HTL process; up to 100 bar and 200 °C to simulate a process integration in an actual HTL plant. Here we used both liquids streams produced by the HTL process, namely biocrude oil and its process water as catholyte and anolyte, respectively. The immiscibility of the two liquid phases allowed us to perform electrolysis experiments in membrane-less configuration, where high ion conductivity of the process water and biocrude resulted in relatively low cell resistances. This together with the benign effect of the high temperature boosted the current density up to 50 mA cm^{-2}, with no mixing in the reactor and thus significant mass-transport limitations. Elemental analysis of the biocrude residue after electrochemical treatment show an increase in the H/C ratio with respect to the pristine biocrude and thermally treated biocrude. FTIR and GC-MS characterization disclosed that the electrochemically treated biocrude composition is in line with the one observed in the ambient pressure low temperature experiments: namely a decrease of ketones and O-containing compounds. While a direct partial hydrogenation of the biocrude can be achieved, we report that the process conditions in terms of temperature, oxygen concentration, mixing and electrical potential difference must be specifically tailored to avoid re-oxidation.

Overall, we demonstrate a *proof-of-concept*, and the results can serve as guidelines for designing and developing next generation electrochemical HTL oil upgrade processes.

CRediT authorship contribution statement

Primavera Pelosin: Methodology, Validation, Formal analysis, Data curation, Writing – original draft, Investigation, Visualization, Project administration, Writing – review & editing. **Francesco Longhin:** Methodology, Validation, Formal analysis, Investigation, Data curation, Writing – review & editing. **Nikolaj Bisgaard Hansen:** Methodology, Software, Validation, Formal analysis, Investigation, Data curation, Writing – review & editing. **Paolo Lamagni:** Methodology, Writing – review & editing. **Emil Drazevic:** Writing – review & editing. **Patricia Benito:** Methodology, Writing – review & editing. **Konstantinos Anastasakis:** Conceptualization, Resources, Supervision, Project administration, Funding acquisition, Writing – review & editing. **Jacopo Catalano:** Conceptualization, Software, Resources, Writing – original draft, Visualization, Supervision, Project administration, Funding acquisition, Writing – review & editing.

Declaration of competing interest

The authors declare that they have no known competing financial interests or personal relationships that could have appeared to influence the work reported in this paper.

Acknowledgements

PP, JC, FL, and KA thank the research grant Villum Experiments from VILLUM FONDEN for generous financial support. PP and JC would like

to thank Marcel Ceccato for his invaluable technical support.

Appendix A. Supplementary data

Supplementary data to this article can be found online at https://doi.org/10.1016/j.renene.2023.119899.

References

[1] S. Fankhauser, et al., The meaning of net zero and how to get it right, Nat. Clim. Change 12 (2022) 15–21.
[2] Renewable energy market update - may 2022 – analysis, IEA, https://www.iea.org/reports/renewable-energy-market-update-may-2022.
[3] Technology needs in long-distance transport – energy technology perspectives 2020 – analysis, IEA, https://www.iea.org/reports/energy-technology-perspectives-2020/technology-needs-in-long-distance-transport.
[4] G. Berndes, M. Hoogwijk, R. van den Broek, The contribution of biomass in the future global energy supply: a review of 17 studies, Biomass Bioenergy 25 (2003) 1–28.
[5] S.N. Naik, V.V. Goud, P.K. Rout, A.K. Dalai, Production of first and second generation biofuels: a comprehensive review, Renew. Sustain. Energy Rev. 14 (2010) 578–597.
[6] K. Anastasakis, P. Biller, R.B. Madsen, M. Glasius, I. Johannsen, Continuous hydrothermal liquefaction of biomass in a novel pilot plant with heat recovery and hydraulic oscillation, Energies 11 (2018) 2695.
[7] Y. Zhu, M.J. Biddy, S.B. Jones, D.C. Elliott, A.J. Schmidt, Techno-economic Analysis of Liquid Fuel Production from Woody Biomass via Hydrothermal Liquefaction (HTL) and Upgrading, vol. 129, 2014, pp. 384–394.
[8] D.C. Elliott, P. Biller, A.B. Ross, A.J. Schmidt, S.B. Jones, Hydrothermal liquefaction of biomass: developments from batch to continuous process, Bioresour. Technol. 178 (2015) 147–156.
[9] P.M. Mortensen, J.D. Grunwaldt, P.A. Jensen, K.G. Knudsen, A.D. Jensen, A review of catalytic upgrading of bio-oil to engine fuels, Appl. Catal. 407 (2011) 1–19.
[10] D. Castello, M.S. Haider, L.A. Rosendahl, Catalytic upgrading of hydrothermal liquefaction biocrudes: different challenges for different feedstocks, Renew. Energy 141 (2019) 420–430.
[11] Z. Wu, R.P. Rodgers, A.G. Marshall, Two- and three-dimensional van Krevelen diagrams: a graphical analysis complementary to the kendrick mass plot for sorting elemental compositions of complex organic mixtures based on ultrahigh-resolution broadband fourier transform ion cyclotron resonance mass measurements, Anal. Chem. 76 (2004) 2511–2516.
[12] J.R. Page, Z. Manfredi, S. Bliznakov, J.A. Valla, Recent progress in electrochemical upgrading of bio-oil model compounds and bio-oils to renewable fuels and platform chemicals, Materials 16 (2023) 394.
[13] Y. Song, et al., Hydrogenation of benzaldehyde via electrocatalysis and thermal catalysis on carbon-supported metals, J. Catal. 359 (2018) 68–75.
[14] N. Singh, et al., Aqueous phase catalytic and electrocatalytic hydrogenation of phenol and benzaldehyde over platinum group metals, J. Catal. 382 (2020) 372–384.
[15] D.A. Giannakoudakis, J.C. Colmenares, D. Tsiplakides, K.S. Triantafyllidis, Nanoengineered electrodes for biomass-derived 5-hydroxymethylfurfural electrocatalytic oxidation to 2,5-furandicarboxylic acid, ACS Sustain. Chem. Eng. 9 (2021) 1970–1993.
[16] Z. Yang, X. Chou, H. Kan, Z. Xiao, Y. Ding, Nanoporous copper catalysts for the fluidized electrocatalytic hydrogenation of furfural to furfuryl alcohol, ACS Sustain. Chem. Eng. 10 (2022) 7418–7425.
[17] W. Xu, C. Yu, J. Chen, Z. Liu, Electrochemical hydrogenation of biomass-based furfural in aqueous media by Cu catalyst supported on N -doped hierarchically porous carbon, Appl. Catal. B Environ. 305 (2022), 121062.
[18] S. Jung, E.J. Biddinger, Controlling competitive side reactions in the electrochemical upgrading of furfural to biofuel, Energy Technol. 6 (2018) 1370–1379.
[19] R. Wu, et al., Electrochemical strategy for the simultaneous production of cyclohexanone and benzoquinone by the reaction of phenol and water, J. Am. Chem. Soc. 144 (2022) 1556–1571.
[20] W. Liu, W. You, Y. Gong, Y. Deng, High-efficiency electrochemical hydrodeoxygenation of bio-phenols to hydrocarbon fuels by a superacid-noble metal particle dual-catalyst system, Energy Environ. Sci. 13 (2020) 917–927.
[21] Z. Li, et al., Mild electrocatalytic hydrogenation and hydrodeoxygenation of bio-oil derived phenolic compounds using ruthenium supported on activated carbon cloth, Green Chem. 14 (2012) 2540.
[22] Z. Li, et al., A mild approach for bio-oil stabilization and upgrading: electrocatalytic hydrogenation using ruthenium supported on activated carbon cloth, Green Chem. 16 (2014) 844–852.
[23] T.E. Lister, et al., Low-temperature electrochemical upgrading of bio-oils using polymer electrolyte membranes, Energy Fuel. 32 (2018) 5944–5950.
[24] W. Deng, et al., Evolution of aromatic structures during the low-temperature electrochemical upgrading of bio-oil, Energy Fuel. 33 (2019) 11292–11301.
[25] T. He, Z. Zhong, B. Zhang, Bio-oil upgrading via ether extraction, looped-oxide catalytic deoxygenation, and mild electrocatalytic hydrogenation techniques, Energy Fuel. 34 (2020) 9725–9733.
[26] X. Yuan, X. Zhu, L. Zhang, Z. Luo, X. Zhu, Fundamental insights into walnut shell bio-oil electrochemical conversion: reaction mechanism and product properties, BioEnergy Res 14 (2021) 322–332.
[27] X. Wang, et al., Coke formation and its impacts during electrochemical upgrading of bio-oil, Fuel 306 (2021), 121664.
[28] R.B. Madsen, et al., Predicting the chemical composition of aqueous phase from hydrothermal liquefaction of model compounds and biomasses, Energy Fuel. 30 (2016) 10470–10483.
[29] P. Biller, et al., Effect of hydrothermal liquefaction aqueous phase recycling on bio-crude yields and composition, Bioresour. Technol. 220 (2016) 190–199.
[30] A. Matayeva, P. Biller, Hydrothermal liquefaction aqueous phase treatment and hydrogen production using electro-oxidation, Energy Convers. Manag. 244 (2021), 114462.
[31] J.A. Lopez-Ruiz, Y. Qiu, E. Andrews, O.Y. Gutiérrez, J.D. Holladay, Electrocatalytic valorization into H2 and hydrocarbons of an aqueous stream derived from hydrothermal liquefaction, J. Appl. Electrochem. 51 (2021) 107–118.
[32] T.H. Seehar, S.S. Toor, A.A. Shah, T.H. Pedersen, L.A. Rosendahl, Biocrude production from wheat straw at sub and supercritical hydrothermal liquefaction, Energies 13 (2020) 3114.
[33] J. Souza dos Passos, A. Matayeva, P. Biiler, Synergies during hydrothermal liquefaction of cow manure and wheat straw, J. Environ. Chem. Eng. 10 (2022), 108181.
[34] S.A. Ansari, N. Parveen, M.A.S. Al-Othoum, M.O. Ansari, Effect of washing on the electrochemical performance of a three-dimensional current collector for energy storage applications, Nanomaterials 11 (2021) 1596.
[35] S. Haldrup, et al., Tailoring membrane nanostructure and charge density for high electrokinetic energy conversion efficiency, ACS Nano 10 (2016) 2415–2423.
[36] R.B. Madsen, et al., Using design of experiments to optimize derivatization with methyl chloroformate for quantitative analysis of the aqueous phase from hydrothermal liquefaction of biomass, Anal. Bioanal. Chem. 408 (2016) 2171–2183.
[37] L.B. Silva Thomsen, et al., Hydrothermal liquefaction of sewage sludge; energy considerations and fate of micropollutants during pilot scale processing, Water Res. 183 (2020).
[38] E. Andrews, et al., Performance of base and noble metals for electrocatalytic hydrogenation of bio-oil-derived oxygenated compounds, ACS Sustain. Chem. Eng. 8 (2020) 4407–4418.
[39] U. Sanyal, J. Lopez-Ruiz, A.B. Padmaperuma, J. Holladay, O.Y. Gutiérrez, Electrocatalytic hydrogenation of oxygenated compounds in aqueous phase, Org. Process Res. Dev. 22 (2018) 1590–1598.
[40] K.J. Carroll, et al., Electrocatalytic hydrogenation of oxygenates using earth-abundant transition-metal nanoparticles under mild conditions, ChemSusChem 9 (2016) 1904–1910.
[41] B. Zhang, J. Zhang, Z. Zhong, Low-energy mild electrocatalytic hydrogenation of bio-oil using ruthenium anchored in ordered mesoporous carbon, ACS Appl. Energy Mater. 1 (2018) 6758–6763.
[42] M.B. Kristensen, A. Bentien, M. Tedesco, J. Catalano, Counter-ion transport number and membrane potential in working membrane systems, J. Colloid Interface Sci. 504 (2017) 800–813. https://doi.org/10.1016/j.jcis.2017.06.010.
[43] M. Garedew, D. Young-Farhat, J.E. Jackson, C.M. Saffron, Electrocatalytic upgrading of phenolic compounds observed after lignin pyrolysis, ACS Sustain. Chem. Eng. 7 (2019) 8375–8386.
[44] O. Derkacheva, D. Sukhov, Investigation of lignins by FTIR spectroscopy, Macromol. Symp. 265 (2008) 61–68.
[45] L. Nazari, Z. Yuan, S. Souzanchi, M.B. Ray, C. (Charles). Xu, Hydrothermal liquefaction of woody biomass in hot-compressed water: catalyst screening and comprehensive characterization of bio-crude oils, Fuel 162 (2015) 74–83.
[46] S. Cheng, I. D'cruz, M. Wang, M. Leitch, C. Xu, Highly efficient liquefaction of woody biomass in hot-compressed Alcohol−Water Co-solvents, Energy Fuel. 24 (2010) 4659–4667.
[47] O. Faix, D.R. L, D. Meier, Direct liquefaction of different lignocellulosics and their constituents, Fuel 65 (1986).
[48] G. Gellerstedt, E.-L. Lindfors, Structural changes in lignin during kraft pulping, Holzforschung 38 (1984) 151–158.
[49] Zhi W. Seh, et al., Combining theory and experiment in electrocatalysis: insights into materials design, Science 355 (2017).
[50] I. Johannsen, B. Kilsgaard, V. Milkevych, D. Moore, Design, modelling, and experimental validation of a scalable continuous-flow hydrothermal liquefaction pilot plant, Processes 9 (2021) 234.
[51] M.J. Muñoz-Portero, J. García-Antón, J.L. Guiñón, R. Leiva-García, Pourbaix diagrams for titanium in concentrated aqueous lithium bromide solutions at 25Â°C, Corrosion Sci. 53 (2011) 1440–1450, 1441.
[52] S. Nagappan, et al., Catalytic hydrothermal liquefaction of biomass into bio-oils and other value-added products – a review, Fuel 285 (2021), 119053.
[53] L.B. Silva Thomsen, K. Anastasakis, P. Biller, Wet oxidation of aqueous phase from hydrothermal liquefaction of sewage sludge, Water Res. 209 (2022), 117863.